

# NJC

Accepted Manuscript



This is an *Accepted Manuscript*, which has been through the Royal Society of Chemistry peer review process and has been accepted for publication.

*Accepted Manuscripts* are published online shortly after acceptance, before technical editing, formatting and proof reading. Using this free service, authors can make their results available to the community, in citable form, before we publish the edited article. We will replace this *Accepted Manuscript* with the edited and formatted *Advance Article* as soon as it is available.

You can find more information about *Accepted Manuscripts* in the [Information for Authors](#).

Please note that technical editing may introduce minor changes to the text and/or graphics, which may alter content. The journal's standard [Terms & Conditions](#) and the [Ethical guidelines](#) still apply. In no event shall the Royal Society of Chemistry be held responsible for any errors or omissions in this *Accepted Manuscript* or any consequences arising from the use of any information it contains.

# Novel 3D flower-like CoNi<sub>2</sub>S<sub>4</sub>/carbon nanotubes composite as high-performance electrode materials for supercapacitor

Zhihong Ai, Zhonghua Hu\*, Yafei Liu, Mengxuan Fan, Peipei Liu

Department of Chemistry, Tongji University, 1239 Siping Road, Shanghai 200092, China

\*Corresponding author. Tel: +86-21-65982594, Fax: +86-21-65982287

Email: huzh@tongji.edu.cn (Z. Hu).

## Abstract:

Novel 3D flower-like CoNi<sub>2</sub>S<sub>4</sub>/carbon nanotubes composites with a porous structure were designed through a facile precursor transformation approach as electrode materials for supercapacitors. The resulting samples are characterized by X-ray diffraction, Raman Spectra, energy dispersive spectroscopy, field emission scanning electron microscopy, transmission electron microscopy, and nitrogen adsorption-desorption. Their electrochemical performance was investigated by means of cyclic voltammetry, galvanostatic charge-discharge, impedance spectra and cycle life. By selecting carbon nanotubes as the conductive support for the growth of CoNi<sub>2</sub>S<sub>4</sub>, the as-obtained CoNi<sub>2</sub>S<sub>4</sub>/carbon nanotubes composites displayed ultrahigh specific capacitance of 2094F g<sup>-1</sup> at 1A g<sup>-1</sup> and good rate capability (72% capacity retention at 10 A g<sup>-1</sup>). These results above suggest the great potential of the unique flower-like CoNi<sub>2</sub>S<sub>4</sub>/carbon nanotubes composites in the development of high-performance electrode materials for supercapacitors.

## Key words:

Nickel cobalt sulfide/carbon nanotubes, Flower-like, Specific capacitance, Supercapacitor

## 1. Introduction

Nowadays, supercapacitors have attracted considerable attention as promising energy storage devices applied in portable electronics, electric or hybrid electric vehicles because of their advantages of fast charge-discharge capability, long lifespan and high energy and power density[1, 2]. Generally, the performance of supercapacitors mainly depends on the properties of their electrode materials. The three types of electrode materials used in the supercapacitors are carbon materials, conductive polymers and metal oxides. Carbon based materials have the advantages in the aspects of abundant resources, high stability and conductivity, but relative low specific capacitance from their electronic double layer capacitance. Conductive polymers have higher specific capacitance than carbons, but poor cycling stability[3]. Transition metal oxides usually possess rich oxidation states that are in favor of a high specific capacitance[4, 5] and the stability is between carbons and conductive polymers; however, their conductivity needs to be further improved. Compared with one component metal oxides NiO and  $\text{Co}_3\text{O}_4$  for example, two components metal oxides, such as spinel  $\text{NiCo}_2\text{O}_4$  owns higher electronic conductivity and more redox reactions could be happened to produce faradic capacitance. However,  $\text{NiCo}_2\text{O}_4$  as electrode material still suffers the disadvantages of slow redox kinetics, poor electrical conductivity and low mechanical stability. In order to solve these problems, highly conductive carbon materials such as active carbon, carbon nanotube(CNT) and graphene are combined with metal oxides to form high performance composite electrode materials, such as NiO/graphene[6],  $\text{MnO}_2/\text{CNT}$ [7],  $\text{V}_2\text{O}_5/\text{CNT}$ [8],  $\text{V}_2\text{O}_5/\text{graphene}$ [9],  $\text{NiCo}_2\text{O}_4/\text{CNT}$ [10, 11],  $\text{NiCo}_2\text{O}_4/\text{graphene}$  [12] and  $\text{RuO}_2/\text{graphene}$ [13].

More recently,  $\text{NiCo}_2\text{S}_4$  is reported to exhibit higher conductivity than  $\text{NiCo}_2\text{O}_4$  owing to the lower optical band gap energy than  $\text{NiCo}_2\text{O}_4$ [14]. Similar with  $\text{NiCo}_2\text{O}_4$ ,  $\text{CoNi}_2\text{S}_4$  is also a binary metallic species and possesses richer valence states than the corresponding

one-component metallic sulfide nickel sulfide (NiS) and cobalt sulfide (Co<sub>9</sub>S<sub>8</sub>)[15]. Chen[14] and his co-workers synthesized urchin-like NiCo<sub>2</sub>S<sub>4</sub> electrode material by a precursor transformation method and the as-obtained product exhibits a high specific capacitance of 1025 F g<sup>-1</sup> at 1 A g<sup>-1</sup>. More recently, Yu et al. synthesized uniform Ni<sub>x</sub>Co<sub>3-x</sub>S<sub>4</sub> hollow nanoprisms[16] with thioacetamide(TAA) as sulfur source. Zhang[17] et al synthesized urchin-, tube-, flower-, and cubic-like NiCo<sub>2</sub>S<sub>4</sub> microstructures through controlling the composition of solvents and found that the solvent polarity and solubility have a significant effect on the process of nucleation and crystal growth. In order to increase the efficient utilization of electrodes, electroactive materials supported by conductive substrates, such as Ni foam[18], graphene[19,20] and carbon cloth[21,22], were also reported. Their electrochemical properties were greatly improved due to the high conductivity, large surface area and three-dimensional network of these substrates. Besides them, carbon nanotube is also highly conductive and has a large surface, in favor of electron transportation and material loading. However, there is not so many reports about the study of the combination of CNT and nickel cobalt sulfides that more works need to be done to in this area, especially in the area of constructing a novel structure through them.

In this work, a new composite electrode material CoNi<sub>2</sub>S<sub>4</sub>/CNT was designed by a two-step route, including the deposition of Co-Ni precursor on CNT and the transformation of the Co-Ni precursor via anion exchange. Before the reaction, CNT was pretreated by acid to increase the amount of oxygen-containing functional groups on the CNT surface in order to improve the deposition of the nickel cobalt precursor on the CNT substrate. In the synthesis process, weak base urea was used as precipitant to control crystal growth of the nickel cobalt precursor in the first step and Na<sub>2</sub>S was taken as the sulfur source for the anion exchange reaction in the second step. The as-obtained CoNi<sub>2</sub>S<sub>4</sub>/CNT composites were characterized by XRD, Raman Spectra, EDS, FESEM, BET and electrochemical tests. The

relation between its unique structure properties and capacitive performance was investigated.

## 2. Experimental

### 2.1 Preparation of CoNi<sub>2</sub>S<sub>4</sub>/CNT composite

Nickel sulfate hexahydrate (NiSO<sub>4</sub> · 6H<sub>2</sub>O), cobalt sulfate heptahydrate (CoSO<sub>4</sub> · 7H<sub>2</sub>O), and urea (CO(NH<sub>2</sub>)<sub>2</sub>) were purchased from Sigma-Aldrich. All reagents are analytical grade. MWCNTs (95% purity, average pore size less than 8nm, length:10–30μm ) were purchased from Timesnano, China. MWCNTs were pretreated by refluxing in 30wt% nitrate acid for 12 h at 100°C. Then the acid-treated CNTs were collected by vacuum filtration and dried at 80 °C for 12 h.

A facile hydrothermal method was used for the synthesis of the Ni-Co sulfide/CNTs composite. Firstly, 4 mmol NiSO<sub>4</sub>·6H<sub>2</sub>O, 2mmol CoSO<sub>4</sub>·7H<sub>2</sub>O and 16 mmol CO(NH<sub>2</sub>)<sub>2</sub> were added into 40 mL DI water and stirred for 30 minutes to form a homogeneous solution. Meanwhile, 40 mg acid-treated CNTs and 15 mg polyvinyl pyrrolidone (PVP) were put in 40 mL ethanol and suffered ultrasonic treatment for 30 min. Then the two solutions were mixed and underwent ultrasonic treatment for 30 minutes. Secondly, the mixture solution was transferred into a Teflon-lined stainless steel autoclave and maintained at 120 °C for 6 h. After cooling down to room temperature, the precursor was separated by centrifugation, washed with DI water and ethanol for several times, and dried at 80 °C for 12h.

0.15 g precursor and 0.54g Na<sub>2</sub>S· 9H<sub>2</sub>O were mixed into 80 ml DI water with vigorous stirring for 30 minutes. Then the mixture was transferred into a 100 ml Teflon-lined stainless steel autoclave and maintained at 160 °C for 12 h. After cooling down, the product was collected and washed with DI water and ethanol for several times, and finally dried at 80 °C.

To study the influence of CNT content on the composite, different CNT amounts 0, 30, 40, 50 and 60 mg were added in the synthesis. The obtained composite samples are denoted as M-0, M-30, M-40, M-50 and M-60, respectively.

## 2.2 Materials characterization

CoNi<sub>2</sub>S<sub>4</sub>/CNTs composite was finally obtained through the above precursor transformation approach. The crystal structure of the composite was studied by X-ray diffraction (XRD, D/max250VB3+/PC, Rigaku) at the scan rate of 1°s<sup>-1</sup> from 10 to 80° with Cu Kα1 radiation). The Raman spectra of the samples was researched by Laser Micro-Raman Spectrometer (Raman, Invia). The morphology was observed by field emission scanning electron microscopy (FESEM, Hitachi S-4800 and JEOL JSM-6060). The elemental compositions were analyzed employing energy dispersive spectroscopy (EDS, 200 kV). The specific surface area and pore size distribution of the prepared samples were estimated according to N<sub>2</sub> adsorption/desorption isotherms at 77 K (Micromeritics, Tristar 3000 gas adsorption analyzer).

## 2.3 Electrochemical measurements

The electrochemical properties of the CoNi<sub>2</sub>S<sub>4</sub>/CNT working electrode were carried out on an electrochemical work station (CHI660C, Chenhua Shanghai) by using a standard three-electrode system. The working electrodes were fabricated by mixing the CoNi<sub>2</sub>S<sub>4</sub>/CNT composite, acetylene black and polytetrafluoroethylene (PTFE) with a weight ratio of 80:10:10 and then adding about 5mL ethanol into the mixture and dispersed in an ultrasonic bath to form a homogeneous paste. Finally, when the ethanol was evaporated, the prepared mixtures were pressed onto a nickel grid under a pressure of 20 MPa for 60 s. 6 mol L<sup>-1</sup> KOH aqueous solution is used as electrolyte; nickel grid and saturated calomel electrode (SCE) served as counter and reference electrode, respectively. The specific capacitance was strictly and carefully calculated from the discharge curves based on the following equation:

$$C_p = \frac{I\Delta t}{\Delta V} \quad (1)$$

where  $C_p$  is the specific capacitance (F g<sup>-1</sup>),  $I$  is the discharging current (A g<sup>-1</sup>),  $\Delta t$  is the

discharge time (s), and  $\Delta V$  is the potential window during the discharge process (V).

### 3. Results and discussion

#### 3.1 Structure characterization and morphology analysis

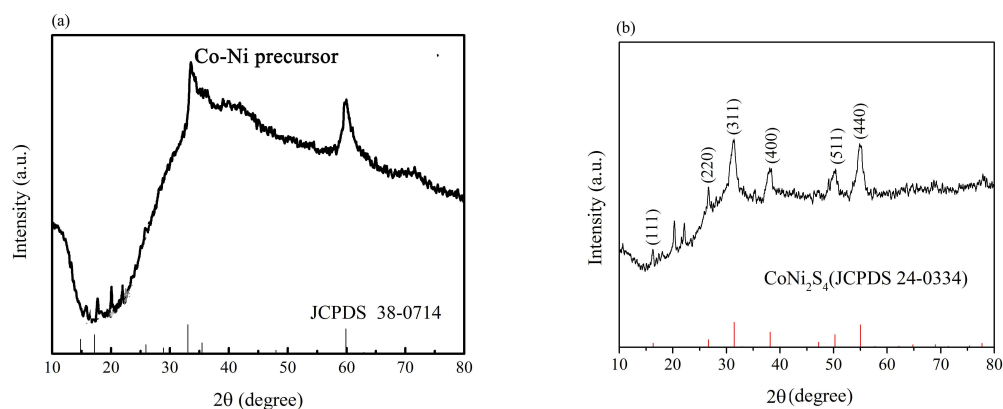


Figure 1 XRD patterns of Co-Ni precursor (a) and final product CoNi<sub>2</sub>S<sub>4</sub>/CNT.

Figure 1a shows the XRD patterns of the precursor. The XRD pattern of the precursor shows nearly the same pattern as that of Ni<sub>2</sub>(OH)<sub>2</sub>CO<sub>3</sub>·4H<sub>2</sub>O, except that all the diffraction peaks slightly shift to the high diffraction direction, in accordance with the fact that Co<sup>2+</sup> or Ni<sup>2+</sup> always forms carbonate hydroxide in a hydrothermal environment in the presence of urea. And this result further suggested that the partial substitution of Ni ions by Co ions does not change the crystal structure except several lattice parameters, owing to the similar atomic radii of Ni and Co [14,17]. After anion exchange reacting with Na<sub>2</sub>S, CO<sub>3</sub><sup>2-</sup> and OH<sup>-</sup> in the precursor nickel cobalt carbonate and hydroxide were gradually replaced by S<sup>2-</sup> and the precursor was chemically converted into its NiCo<sub>2</sub>S<sub>4</sub>/CNT counterpart.

Figure 1b shows the XRD patterns of the as-prepared CoNi<sub>2</sub>S<sub>4</sub>/CNT sample. The characteristic peaks at 16.3°, 26.7°, 31.5°, 38.2°, 47.4°, 50.3° and 55.0° respectively correspond to (111), (220), (311), (400), (511) and (440) planes of the cubic CoNi<sub>2</sub>S<sub>4</sub> phase (JCPDS Card No.24-0334). Besides, the two weak peaks in the range between 20° and 25° is believed to be caused by the acid-treated CNT which always has a typical peak at 26° [23, 24].

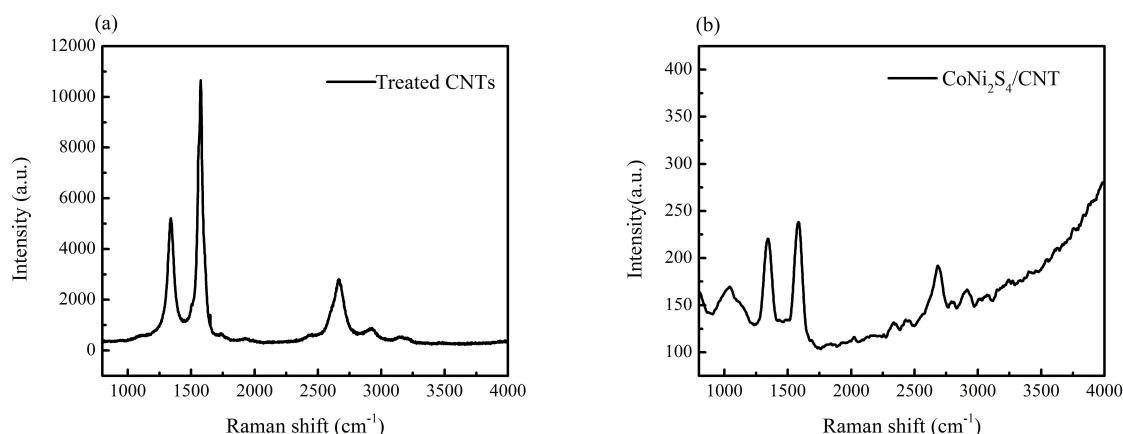


Figure 2 Raman spectra of the acid-treated CNTs (a) and the  $\text{CoNi}_2\text{S}_4/\text{CNTs}$  composites(b).

Figure 2 presents the Raman spectra of the pure acid-treated carbon CNTs and the  $\text{CoNi}_2\text{S}_4/\text{CNTs}$  composites in the range from 800 to 4000  $\text{cm}^{-1}$ . Three typical graphic peaks can be seen both in the Raman spectra of the pure acid-treated carbon CNTs and the  $\text{CoNi}_2\text{S}_4/\text{CNTs}$  composites: the peak at 1348  $\text{cm}^{-1}$ , D band, owes to the breathing modes of rings or  $\kappa$ -point photons of  $A_{1g}$  symmetry, the symbol of the defects on the CNTs surface[25]; the peak at 1585  $\text{cm}^{-1}$ , G band, owes to the splitting  $E_{2g}$  stretching mode of graphite; the peak at 2086  $\text{cm}^{-1}$ , 2D band, results from a harmonic of the D band[26]. These two Raman spectroscopies give a good demonstration about the existence of CNTs in the composites.

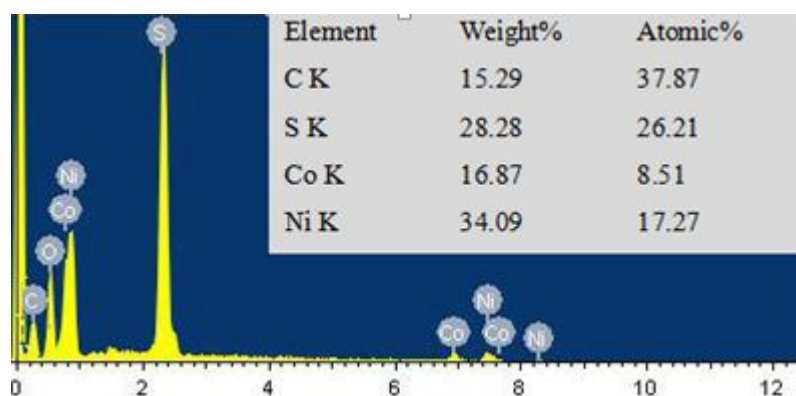


Figure 3 EDS spectrum of the  $\text{CoNi}_2\text{S}_4/\text{CNT}$  sample.

The EDS spectrum proves the existence of Co, Ni, S, C and O elements in the  $\text{CoNi}_2\text{S}_4/\text{CNT}$  sample as shown in Fig. 3. The element molar ratio of Co and Ni is 1:2.03, which is very close to the ratio of Ni and Co atom in the formula of  $\text{CoNi}_2\text{S}_4$ . Noticeably, the

content of C is 37.87%, including both the slight C in the substrate and other C in the CNTs. The O element is supposed to come from oxygen functional groups on the surface of CNTs or the residual oxygen atom, because of incomplete sulfur treatment.

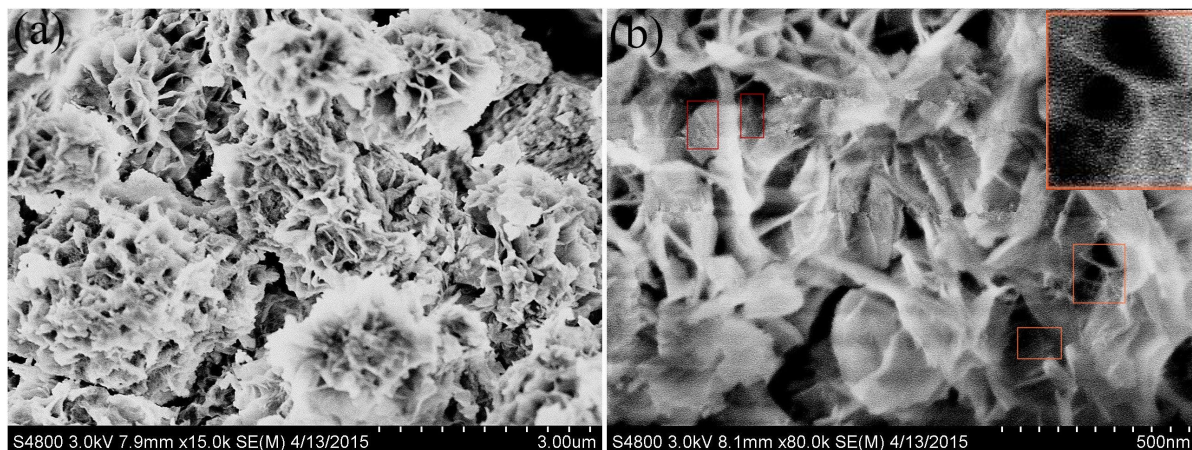


Figure 4 FESEM images of the Co-Ni precursor.

The morphological features of the  $\text{CoNi}_2\text{S}_4$  /CNT samples were studied by FESEM, as shown in Fig. 4. Fig. 4(a,b) displays the FESEM image of the precursor, which appears to be 3D flower-like structures with a diameter of approximately  $2 \mu\text{m}$  and composed of lots of interconnected nanosheet about 10 nm thick. Besides, it can be found that the MWCNTs (short and tiny rods) are partly enwrapped in the nanosheet and partly lie between nanosheets, as shown in the red rectangle in the high-magnification image of Fig. 4 b., in favor of forming the basic 3D flower texture of the flower structure. And the shape was well preserved after sulfidation as can be seen in Fig. 5a.

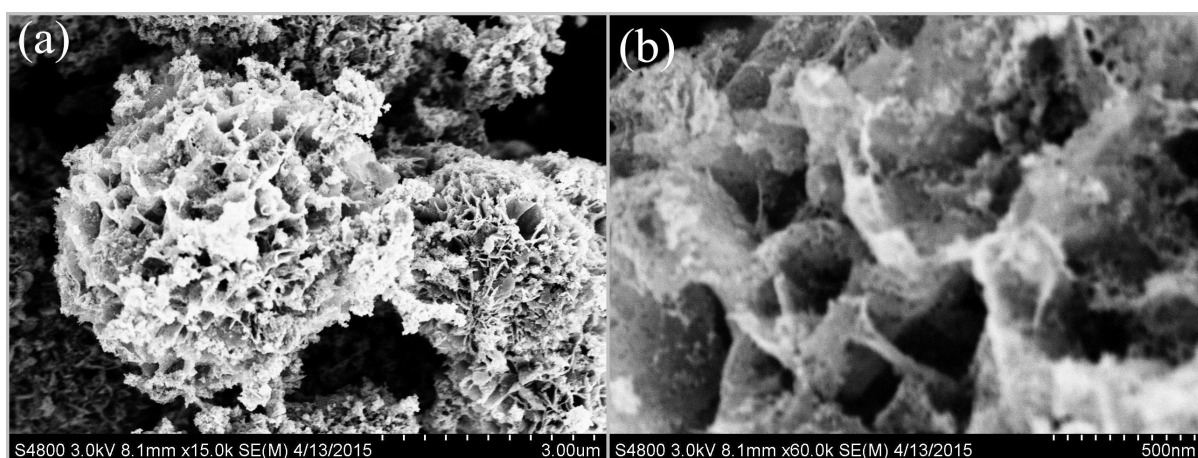


Figure 5 FESEM images of  $\text{CoNi}_2\text{S}_4$  /CNT.

Moreover, it can be observed that the surface of the nanosheets became rather rough and porous, as shown in the high-magnification images of Fig. 5b. Here, it is worthwhile to point out that in the process of crystal growth, PVP, a non-ionic surfactant, could induce faces toward different directions to grow with different speed and lead to the final flower-like structure.

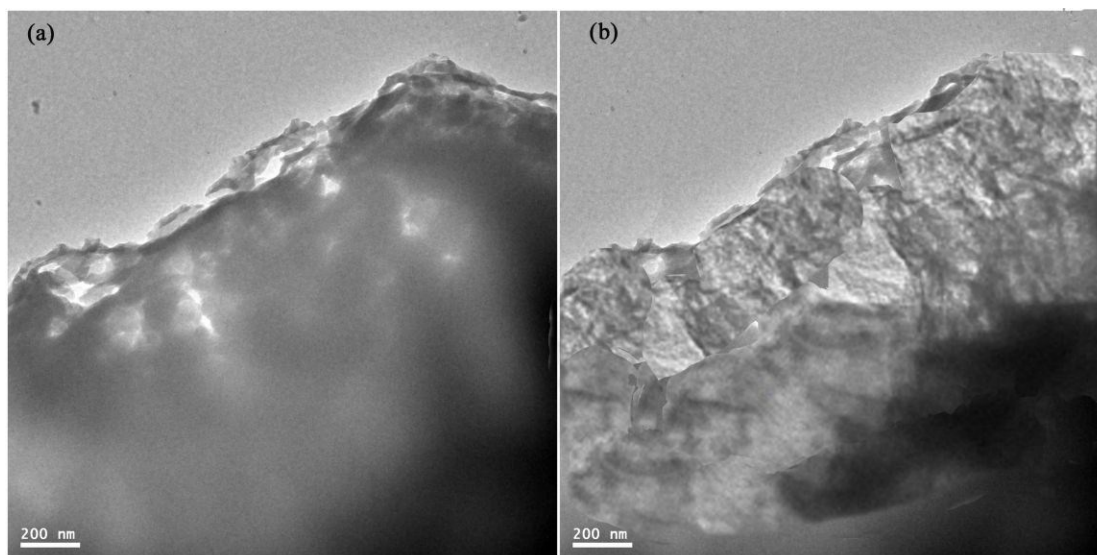


Figure 6 TEM images of CoNi<sub>2</sub>S<sub>4</sub>(a) and CoNi<sub>2</sub>S<sub>4</sub>/CNT(b).

Besides, the TEM characterization CoNi<sub>2</sub>S<sub>4</sub>(a) and CoNi<sub>2</sub>S<sub>4</sub>/CNT are also done, as can be seen in Fig. 6. The edges of their nanosheets are presented and compared. There seems to be many slim rods in the nanosheet of CoNi<sub>2</sub>S<sub>4</sub>/CNT, which is a symbol of the existence of CNT in the sample. But the lattice spacing was not given due to its weak crystallinity, which is in accordance with the XRD characterization result.

### 3.2 Electrochemical properties

The cyclic voltammetry (CV), galvanostatic charge-discharge and electrochemical impedance spectroscopy (EIS) were measured in order to investigate the electrochemical properties of the as-obtained CoNi<sub>2</sub>S<sub>4</sub>/CNTs composites as shown in Fig 5.

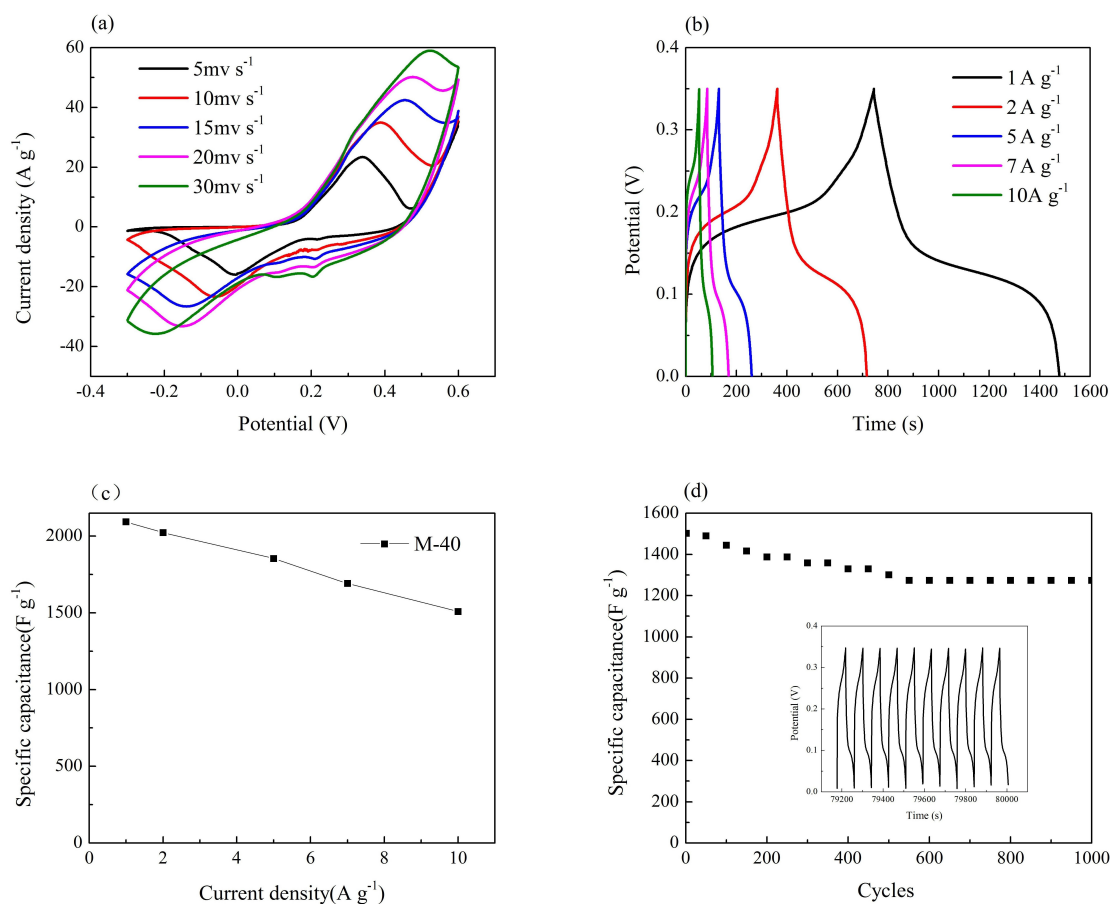


Figure 7 Electrochemical test results of M-40 electrode. (a) CV curves; (b) galvanostatic charge-discharge tests ; (c) specific capacitance as a function of discharge current density; (d) cycling stability of 1000-cycles charge-discharge at 10 A g<sup>-1</sup> (the insert shows the last 10 cycles).

Fig. 7a shows the oxidation and reduction peaks can be clearly observed in the potential range of -0.3-0.6V, suggesting the good pseudocapacitive characteristics. With the scan rate increasing from 5 mV s<sup>-1</sup> to 30 mV s<sup>-1</sup>, the anode peak shifts to a higher potential and the cathodic peak shifts to a lower potential. And more peaks appear around 0.2V, which may result from the abundant Faradic redox processes of Ni<sup>2+</sup>/Ni<sup>3+</sup> and Co<sup>2+</sup>/Co<sup>3+</sup>/Co<sup>4+</sup> transitions associated with anions OH<sup>-</sup>. The redox reactions in the alkaline electrolyte are based on the following mechanism[27]:





The distortion of the CV curves becomes more and more serious as the scan rate increases from 5 mV s<sup>-1</sup> to 30 mV s<sup>-1</sup>. It's because the ionic diffusion rate in the case of high scan rate was not fast enough to satisfy electronic neutralization during the redox reactions.

Fig. 7b shows the galvanostatic charge–discharge curves of the CoNi<sub>2</sub>S<sub>4</sub> /CNTs electrode within the potential window between 0 and 0.35 V at the discharge current density of 1, 2, 5, 7 and 10 A g<sup>-1</sup>, respectively. The shape of charge–discharge curves exhibits a typical pseudocapacitive behavior. Encouragingly, for M-40, the specific capacitance values are as high as 2094, 2022, 1855, 1694 and 1510 F g<sup>-1</sup> at current densities of 1, 2, 5, 7 and 10 A g<sup>-1</sup>, respectively, as shown in Fig. 7c, which is much higher than that of other NiCo<sub>2</sub>S<sub>4</sub> or CoNi<sub>2</sub>S<sub>4</sub> materials reported in the literature as listed in Table 1. The higher capacitance of CoNi<sub>2</sub>S<sub>4</sub> /CNTs electrode probably stemmed from its novel 3D flower-like structure with many pores formed between interconnected nanosheets, which got a high efficiency of the space and provided enough active sites for electrochemical reaction with electrolytes.

Table 1 Specific capacitance and capacitive retention of CoNi<sub>2</sub>S<sub>4</sub> materials from literatures and prepared in this work

Sample	Specific capacitance (F g <sup>-1</sup> /1A g <sup>-1</sup> )	Rate retention (%)	Current Range (A g <sup>-1</sup> )	BET (m <sup>2</sup> g <sup>-1</sup> )	Reference
Urchin-like NiCo <sub>2</sub> S <sub>4</sub>	1025	77.3	1-20	/	[14]
CoNi <sub>2</sub> S <sub>4</sub> /graphene	2009	49.8	1-20	48.4	[28]
Nanostructured NiCo <sub>2</sub> S <sub>4</sub>	1050	66.2	1-50	20.3	[18]
NiCo <sub>2</sub> S <sub>4</sub> hollow nanoprisms	895	65.4	1-20	30.0	[16]
NiCo <sub>2</sub> S <sub>4</sub> nanotubes	933	58.9	1-5	32.0	[29]
NiCo <sub>2</sub> S <sub>4</sub> nanosheets on graphene	1300 (3A g <sup>-1</sup> )	52.3	3-20	79.1	[20]
Porous NiCo <sub>2</sub> S <sub>4</sub> hexagonal nanoplates	966	95.5	1-10	17.4	[30]
CoNi <sub>2</sub> S <sub>4</sub> nanoparticles	1169	60.1	1-5	21.6	[18]
Mesoporous NiCo <sub>2</sub> S <sub>4</sub> nanoparticles	972 (2A g <sup>-1</sup> )	86.8	2-20	42.8	[31]
Ball-in-ball hollow NiCo <sub>2</sub> S <sub>4</sub> spheres	1036	68.1	1-20	/	[32]
Hollow tubular NiCo <sub>2</sub> S <sub>4</sub>	1046(2A g <sup>-1</sup> )	68.0	2-20	108.4	[33]
3D flower-like CoNi <sub>2</sub> S <sub>4</sub>	2094	72.0	1-10	31.5	Our work

Cycle stability is also an important factor determining the electrochemical performance of the electrode materials. In the present work, cycle stability experiments were carried out at the charge-discharge current density of 10 A g<sup>-1</sup> in the potential range of 0–0.35 V for 1000 repetitive cycles, as shown in Fig. 7 (d). The specific capacitance loss after 1000 cycles was 16%, suggesting that the capacity retention was as high as 84%. The last 10 cycles were presented as insert. It was found that the shapes of the charge–discharge curves were nearly unchanged, indicating the good reversibility and cyclic life of CoNi<sub>2</sub>S<sub>4</sub> /CNTs electrodes.

### 3.3 The influence of the CNTs added in the composite on the electrochemical property

The nitrogen adsorption-desorption and electrochemical tests were measured in order to investigate the influence of different CNTs amounts added in the composite on the properties of the final samples.

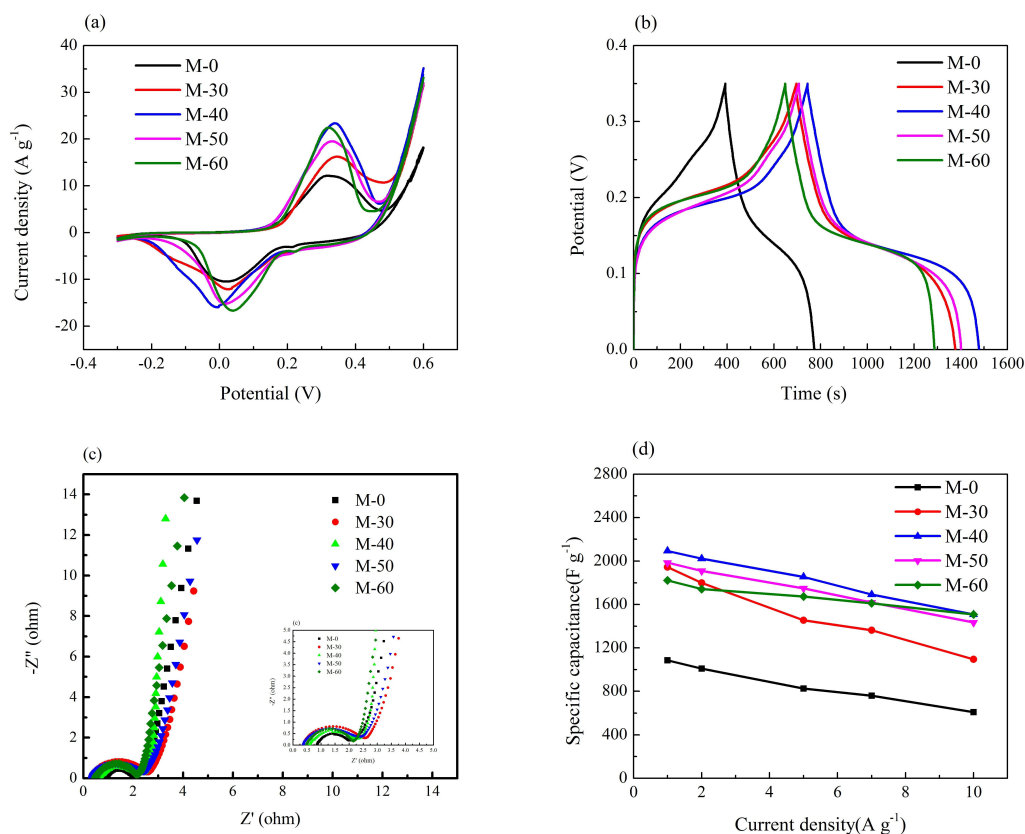


Figure 8 (a) CVs; (b) charge-discharge curves; (c) impedance spectra; (d) specific change with different current density of the samples M-0, M-30, M-40, M-50, M-60.

Fig. 8 (a) shows the typical CV curves of M-0, M-30, M-40, M-50, and M-60 at the scanning rate of  $5 \text{ mV s}^{-1}$  in the potential range from  $-0.3 \text{ V}$  to  $0.6 \text{ V}$ . Evidently, M-40 has the largest CV area, meaning that the M-40 electrode got the highest specific capacitance. The specific capacitance of the composite electrodes increases with increasing CNT addition from  $0 \text{ mg}$  to  $40 \text{ mg}$ , but decreases from  $40 \text{ mg}$  to  $60 \text{ mg}$ . Thus the addition of  $40 \text{ mg}$  of CNTs in the composite is the optimal value. The galvanostatic charge-discharge at  $1 \text{ A g}^{-1}$  in a potential window of  $0\text{--}0.35 \text{ V}$  is shown in Fig. 8 (b). The sample M-40 exhibits the longest discharge time, suggesting that it has the highest specific capacitance. Reasonably, it's because the synergistic effect of the pseudocapacitance of  $\text{CoNi}_2\text{S}_4$  and the double-layer capacitance of CNTs[34]. But when the content of CNTs exceeds  $40 \text{ mg}$ , the double-layer capacitance of CNTs has a greater effect on the electrodes than the pseudocapacitance of

CoNi<sub>2</sub>S<sub>4</sub> so that the capacitance decreased instead.

The test result of electrochemical impedance spectroscopy(EIS) is shown in Fig. 8 (c), all EIS curves have similar shape consisting of a semicircle on the left and a inclined line on the right. Among them, the inclined line of M-40 in the low frequency region are almost parallel to the vertical axis, which means the Warburg resistance is rather small and the fast ion-diffusion behavior in the electrolyte. The change of capacitance with the increasing current density, also called rate capacity, is another important factor other than specific capacitance and cycle life. As shown in Fig. 8(d), when the current density changes from 1A g<sup>-1</sup> to 10A g<sup>-1</sup>, the capacitance retention of M-0, M-30, M-40, M-50, and M-60 are 56%, 57%, 72%, 73%, 83%, respectively. Interestingly, the rate capacity was improved with the increasing amount of CNT, which may due to the increasing conductivity that facilitates access for electron transfer and benefits the fast charging and discharging[14].

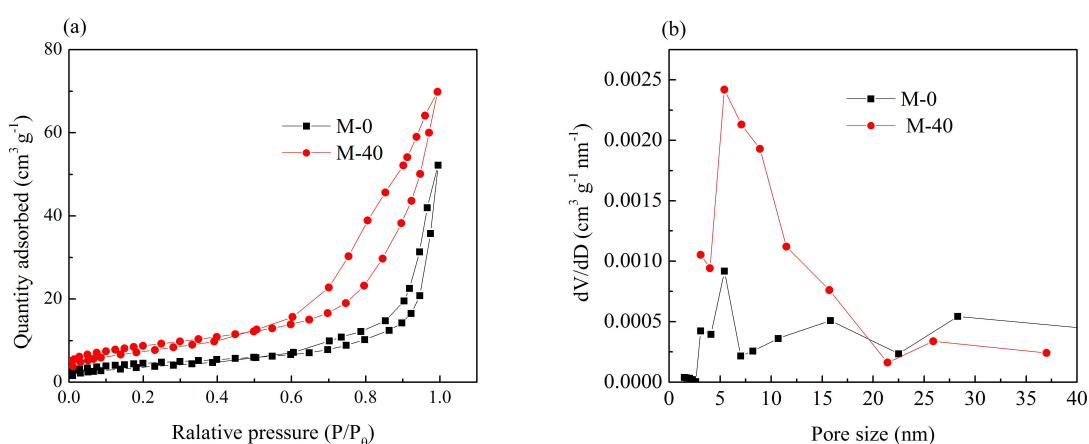


Figure 9 (a) Nitrogen adsorption-desorption isotherms and (b) corresponding pore size distributions of M-0 and M-40.

The BET characterization was carried out to investigate the specific surface area and pore-size distribution of the as-prepared samples. The adsorption/desorption isotherms are of the combination of the Type I and Type V isotherms as shown in Fig. 9(a), and with a typical H3 hysteresis loop, suggesting the presence of mesopores for CoNi<sub>2</sub>S<sub>4</sub>/CNTs composite

samples M-0 and M-40. Their pore size distributions are shown in Fig. 9(b). It is clear that that most pores are in the range of 4–15 nm. The mesoporous structure possibly came from the slot pores[35] between the interconnected nanosheets in the flower structure.

The specific surface area, pore volume and average pore size details are listed in Table 2.

Table 2. Specific surface area, pore volume and average pore size of CoNi<sub>2</sub>S<sub>4</sub>/CNTs composite samples.

Samples	S <sub>BET</sub> (m <sup>2</sup> .g <sup>-1</sup> )	V <sub>tot</sub> (cm <sup>3</sup> .g <sup>-1</sup> )	PS(nm)
M-0	16.2	0.081	19.9
M-40	31.5	0.108	13.7

S<sub>BET</sub>, BET specific surface area; V<sub>tot</sub>, total pore volume; PS, average pore size

It is noteworthy to point out that the specific area of M-40 was much larger and the average pore size became smaller than that of M-0. The improved specific surface area can be attributed to its hierarchical structure with CNTs embedded in and between sheets consisting of the flower structure, which is beneficial to the mass and charge transport during the electrode reaction. Besides, the average pore size of M-40 shifted to a smaller one than that of M-0, leading to the higher specific surface area and more active sites for electrochemical reactions. Thus both improved specific area and reasonable mesopore size distribution are responsible for the enhanced electrochemical properties.

#### 4. Conclusion

3D flower-like CoNi<sub>2</sub>S<sub>4</sub>/carbon nanotubes composite was synthesized by a facile Co-Ni precursor transformation route via anion exchange with Na<sub>2</sub>S. It exhibits ultrahigh specific capacitance of 2094 F g<sup>-1</sup> at 1A g<sup>-1</sup> and high capacity retention rate of 72% when discharge current density increased by ten times from 1 A g<sup>-1</sup> to 10 A g<sup>-1</sup>. Additionally, desirable cycling stability (83.4% of the initial capacity retention after 1000 cycles at 10 A g<sup>-1</sup>) was achieved. Such outstanding capacitive behaviors of the CoNi<sub>2</sub>S<sub>4</sub>/carbon nanotubes composite are mainly ascribed to the rich redox reactions that contribute from both nickel and cobalt

ions, high conductivity of carbon nanotube, novel 3D flower-like structure and optimal mesopore size. The novel  $\text{CoNi}_2\text{S}_4$ /carbon nanotubes composite could be a promising electrode material for high-performance supercapacitors.

### **Acknowledgments**

This work is supported by Tongji University Research Foundation (1380219039).

**Reference:**

- [1] D. P. Dubal, P. Gomez-Romero, B. R. Sankapal and R. Holze, *Nano Energy*, 2015, **11**, 377.
- [2] L. Yu, H. Wu, T. Wu and C. Yuan, *RSC Adv.*, 2013, **3**, 23709.
- [3] H. Chen, J. Jiang, L. Zhang, D. Xia, Y. Zhao, D. Guo, T. Qi and H. Wan, *J. Power Sources*, 2014, **254**, 249.
- [4] F. Cao, G.X. Pan, X. H. Xia, P.S. Tang and H. F. Chen, *J. Power Sources*, 2014, **264**, 161.
- [5] Y. Wang, A. Pan, Q. Zhu, Z. Nie, Y. Zhang, Y. Tang, S. Liang and G. Cao, *J. Power Sources*, 2014, **272**, 107.
- [6] X. Feng, J. Zhou, L. Wang, Y. Li, Z. Huang, S. Chen, Y. Ma, L. Wang and X. Yan, *New J. Chem.*, 2015, **39**, 4026.
- [7] L. Chen, Y. Zhou, H. Dai, T. Yu, J. Liu and Z. Zou, *Nano Energy*, 2015, **11**, 697.
- [8] I. Shakir, Z. Ali, J. Bae, J. Park, and D. J. Kang, *Nanoscale*, 2014, **6**, 4125.
- [9] F. Cai, Y. Kang, H. Chen, M. Chen and Q. Li, *J. Phys. Chem. A*, 2014, **2**, 11509.
- [10] I. Shakir, *Electrochim. Acta*, 2014, **132**, 490.
- [11] X. Wang, X. Han, M. Lim, N. Singh, C. L. Gan, M. Jan and P. S. Lee, *J. Phys. Chem. C*, 2012, **116**, 12448.
- [12] E. Mitchell, A. Jimenez, R. Gupta, B. K. Gupta, K. Ramasamy, M. Shahabuddin and S. R. Mishra, *New J. Chem.*, 2015, **39**, 2181.
- [13] Y. Yang, Y. Liang, Y. Zhang, Z. Zhang, Z. Li and Z. Hu, *New J. Chem.*, 2015, **39**, 4035.
- [14] H. Chen, J. Jiang, L. Zhang, H. Wan, T. Qi and D. Xia, *Nanoscale*, 2013, **5**, 8879.
- [15] J. Xiao, L. Wan, S. Yang, F. Xiao and S. Wang, *Nano letters*, 2014, **14**, 831.
- [16] L. Yu, L. Zhang, H. B. Wu and X. W. Lou, *Angew. Chem.*, 2014, **53**, 3711.

- [17] Y. Zhang, M. Ma, J. Yang, C. Sun, H. Su, W. Huang and X. Dong, *Nanoscale*, 2014, **6**, 9824.
- [18] W. Du, Z. Zhu, Y. Wang, J. Liu, W. Yang, X. Qian and H. Pang, *RSC Adv.*, 2014, **4**, 6998.
- [19] S. Peng, L. Li, C. Li, H. Tan, R. Cai, H. Yu, S. Mhaisalkar, M. Srinivasan and S. Ramakrishna, Q. Yan, *Chem. commun.*, 2013, **49**, 10178.
- [20] J. Tang, J. Shen, N. Li and M. Ye, *Ceram. Int.*, 2015, **41**, 6203.
- [21] M. Sun, J. Tie, G. Cheng, T. Lin, S. Peng, F. Deng, F. Ye and L. Yu, *J. Mater. Chem. A*, 2015, **3**, 1730.
- [22] S. Liu, Y. Liu, W. Song, J. Song, C. Wang, G. Shao and X. Qin, *J. Solid State Electrochem.*, 2015, **19**, 1321.
- [23] H. Cheng, A. D. Su, S. Li, S. T. Nguyen, L. Lu, C. Y. H. Lim and H. M. Duong, *Chem. Phys. Lett.*, 2014, **601**, 168.
- [24] Z. Tang, C. Tang and H. Gong, *Adv. Funct. Mater.*, 2012, **22**, 1272.
- [25] X. Wang, X. Han, M. Lim, N. Singh, C. L. Gan, M. Jan and P. S. Lee, *J. Phys. Chem. C*, 2012, **116**, 12448.
- [26] M.S. Dresselhaus, G. Dresselhaus, R. Saito and A. Jorio, *Phys. Rep.*, 2005, **409**, 47.
- [27] T. Zhu, Z. Wang, S. Ding, J.S. Chen and X.W. Lou, *RSC Adv.*, 2011, **1**, 397.
- [28] W. Du, Z. Wang, Z. Zhu, S. Hu, X. Zhu, Y. Shi, H. Pang and X. Qian, *J. Mater. Chem. A*, 2014, **2**, 9613.
- [29] H. Wan, J. Jiang, J. Yu, K. Xu, L. Miao, L. Zhang, H. Chen and Y. Ruan, *CrystEngComm*, 2013, **15**, 7649.

- [30] J. Yang, W. Guo, D. Li, Q. Qin, J. Zhang, C. Wei, H. Fan, L. Wu and W. Zheng, *Electrochim. Acta*, 2014, **144**, 16.
- [31] Y. Zhu, Z. Wu, M. Jing, X. Yang, W. Song and X. Ji, *J. Power Sources*, 2015, **273**, 584.
- [32] L. Shen, L. Yu, H. B. Wu, X.Y. Yu, X. Zhang, X. W. Lou, *Nat. Commun.*, 2015, **6**, 6694.
- [33] Y. M. Chen, Z. Li and X. W. Lou, *Angew. Chem. Int. Ed.*, 2015, **54**, 10521.
- [34] P. Liu, Z. Hu, Y. Liu, M. Yao and Q. Zhang, *J. Alloys Compd.*, 2015, **622**, 805.
- [35] D. Du, Z. Hu, Y. Liu, Y. Deng and J. Liu, *J. Alloys Compd.*, 2014, **589**, 82.

### Graphical Abstract

Mesoporous  $\text{CoNi}_2\text{S}_4/\text{CNT}$  compounds prepared by a precursor transformation method displayed excellent capacitance performance.

